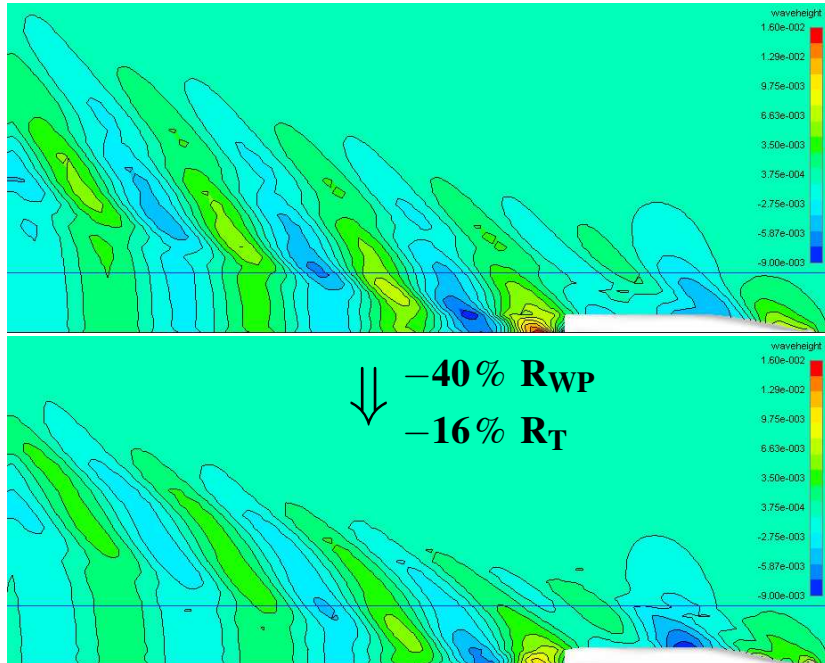


# CFD - based Optimization of the Wave-Making Characteristics of Ship Hulls

## CFD - basierte Optimierung der wellenbildenden Eigenschaften schneller Schiffe

Justus Heimann, FRIENDSHIP SYSTEMS GmbH, Heimann@FRIENDSHIP-SYSTEMS.com



### Abstract

Ship optimization based on computer simulations has become a decisive factor in the development of new, economically efficient and environmentally friendly ship hull forms. An important task at an early design stage is the optimization of the wave-making characteristics of the ship hull since a considerable resistance component stems from the steady ship wave system. Moreover, the ship waves cause adverse effects in the far field as the wash hits the shore line or other vessels.

A novel hull form optimization approach is presented. It builds on a CFD (Computational Fluid Dynamics) based evaluation of the ship wave pattern, on straightforward realization of the cause and effect relation of hull variations and their impact on wave formation, which is accessed by a perturbation approach, and on wave cut analysis. Wave cut analysis yields an excellent assessment of the wave-making characteristics of a hull form in terms of its free wave spectrum and

the associated resistance. These features are highly integrated and controlled by a fully automated, self-governed optimization scheme used to improve the wave-making characteristics accompanied by a substantial reduction of the ship's resistance and power consumption.

*Die Entwicklung ökonomisch und ökologisch effizienter Schiffe erfordert im großem Maße den Einsatz moderner, rechnergestützter Verfahren. Eine ausschlaggebende Rolle hierbei spielt die auf Computersimulationen basierende hydrodynamische Optimierung des Schiffsrumpfes. Ein erheblicher Teil des Rumpfwiderstandes und damit des Leistungsbedarfs wird durch Energieverluste infolge der Ausbildung des Schiffswellensystems verursacht. Zudem gefährden Schiffswellen Küstenschutzmaßnahmen, Uferbebauungen, die Ufervegetation, Hafenanlagen und andere Schiffe.*

*Es wird ein neuartiger Optimierungsansatz vorgestellt, der sich auf die Wellenbildungseigen-*

*schaften von Schiffsrümpfen konzentriert. Das Verfahren beruht auf der rechnergestützten Simulation des Schiffswellenfeldes, auf der Betrachtung des Ursache-Wirkungs-Zusammenhanges von Rumpfvibrationen und deren Auswirkung auf die Wellenbildung mittels eines Perturbations-schemas sowie auf der Wellenschnittmethodik, die ein nützliches Instrument für die Bewertung der Wellenbildungseigenschaften von Rumpf-geometrien liefert. Diese Bausteine wurden zu einem voll automatischen, autonom arbeitenden Optimierungssystem integriert, mit dem sich die Wellenbildung und damit Widerstand und Leistungsbedarf substantiell verringern lassen.*

## 1 Introduction

The recent boom in the global trade calls for a new fleet of ships being at the cutting-edge of technical innovation and ecological standards. The increasing size and speed of recent cargo vessels like the new ultra-large container ships in combination with ever higher fuel prices demand for extra effort in improving the hull hydrodynamics. This extra effort pays-off economically and ecologically in short-term for shipowner and/or operators due to reduced ship operating costs, preserved or even shortened turn around times and less emissions, see Harries et al. (2006).

From a techno-economically point of view hydrodynamic hull form optimization may pursue the following goals:

- Lower resistance and power consumption for same payload (and/or stability) and speed,
- increased speed for constant power consumption and payload,
- more payload for about the same power consumption and speed,
- reduced draft for comparable payload,
- without impairing operational and construction aspects.

The key aspect to meet one or more of these optimization goals is the reduction of the ship's resistance. A considerable resistance component stems from the steady ship wave system. Fast displacement type ships consume 50% and above of their installed power to overcome the wave resistance. The

ship waves may also cause serious (environmental) damages as the wash hits the shore line, other vessels or harbor and offshore installations as, e.g., outlined by a representative study of the environmental impact of a catamaran ferry wake wash in San Francisco Bay, see Kumar et al. (2006). For this reasons it is mandatory to reduce wave-making as much as possible.

Due to the availability of fast and increasingly reliable CFD codes, in particular free surface Rankine panel codes (computation of the viscous free surface flow for the full scale ship by a RANSE code is extremely costly and, hence, prohibitive for automatic optimization), advanced CASHD (Computer Aided Ship Hull Design) tools for the geometric hull modeling and a wide range of suitable optimization methods, hydrodynamic ship optimization has become a rapidly developing field of both research and practical application. Tools range from fully automatic implementations over semi-interactive environments to highly interactive optimization approaches. The latter are still favored by many shipyards and model basins and often involve EFD (Experimental Fluid Dynamics). Related CFD-based hull form optimizations with particular focus on wave resistance reduction were reported more recently, e.g., by Birk and Harries (2000), Söding (2001), Heimann and Harries (2003), Maisonneuve et al. (2003), Valdenazzi et al. (2003), Valorani et al. (2003), Dudson and Harries (2005), Heimann (2005) and Harries et al. (2006) (for a more complete list see Heimann (2005)).

This paper represents a novel optimization approach which differs from other approaches to wave resistance minimization in the way it tackles this objective. The potential of the method is substantiated by two exemplary ship applications: an academic test case – the standard Wigley hull – and a state of the art twin screw ferry – the FANTASTIC FantaRoRo – typical of fast short-sea shipping featuring a bulbous bow and tunneled transom stern. A substantial reduction of the ship's wave-making was achieved, an impression is given in title figure.

All aspects of the proposed optimization approach are presented. The main achievements and contributions of the present work are summarized and an outlook to present research work is given.

For a thorough description of the optimization method the reader is referred to Heimann (2005).

## 2 Hydrodynamic optimization

A fully automated, self-governed hull form optimization environment called MinSWASH (Minimum Ship Wash) has been developed and implemented by the author, see Heimann (2005). It controls the optimization process flow, it comprises a sensitivity analysis, the optimization kernel and a wave cut analysis scheme, and it establishes the connection to the nonlinear free surface Rankine panel module of the SHIPFLOW system by FLOWTECH Int. AB.

The key aspects of the optimization approach are:

- Different from common practise neither prerequisites to the hull geometry representation and its characteristic features nor to the hull variation method need to be imposed since
- optimization control is attained via a flow related quantity, being the hull panel source densities of potential flow, so called perturbators, which serve as
- locally operating optimization variables ( $N > 10^3$ ) working directly
- at the wetted hull portion of the advancing ship in it's dynamic floating position.
- The objective function of optimization is directly related to the steady ship wave systems in terms of the free wave spectra and the wave-making resistance as determined by longitudinal wave cut analysis which proved to be a robust assessment method.
- Compared to purely scalar resistance values like integrated hull pressure wave pattern analysis improves the system identification by tracing hull variations up to their respective fingerprints in the wave spectral distribution and in the wave pattern resistance.
- The boundary value problem of nonlinear potential free surface flow is accessed by linear perturbation. Thus, fast and straightforward evaluation of the sensitivities of the objective function and the constraints is enabled, allowing a simultaneous treatment of numerous, locally acting optimization variables which introduces a high degree of freedom to the hull variation.
- The optimization process is effectively established in terms of an iterative marching scheme of successive sub-optimization loops which built

on top of each other, each mapping the solution space to a simplified convex quadratic image, i.e., the sub-optimization space in a 'trust-region' around the current base point, which merely possesses a single minimum determined by the active constraints.

- The entire process is self-sufficient requiring no user interaction at all and only minor preparations.

This particular optimization concept was conceived to pursue the following goals:

- Optimization of the wave-making characteristics, i.e., tangible reduction of the wave pattern resistance of the hull at its dynamic floating position.
- Self-adjusting hull geometry variation, driven directly and solely by the hydrodynamic optimization.
- Concerted reduction of particular adverse wave components and realization of optimal interfering wave trains.
- Acquisition of knowledge of the correlation between local hull shape and wave formation.

### 2.1 Process flow

The optimization process flow is shown in figure 1. A full sub-optimization task is performed by processing the flow chart once. Normally, a series of sub-optimization tasks is conducted by progressively reentering the loop (follow the upward link at the right hand side).

Within the optimization environment five stages are highly integrated setting up a complete sub-optimization task:

**Initial quality assessment** The optimization process commences with the initial (or an intermediate quality assessment when the process progresses) quality assessment. At this stage the process control parameters and the hull geometry enter the process. Control parameters concern the global process flow, the sensitivity analysis, the free surface flow simulation, the wave cut analysis and the set-up and solution of the minimization problem. The hull geometry is given in terms of an initial offset or panel input point mesh. An initial nonlinear free surface flow computation is performed which is forced to

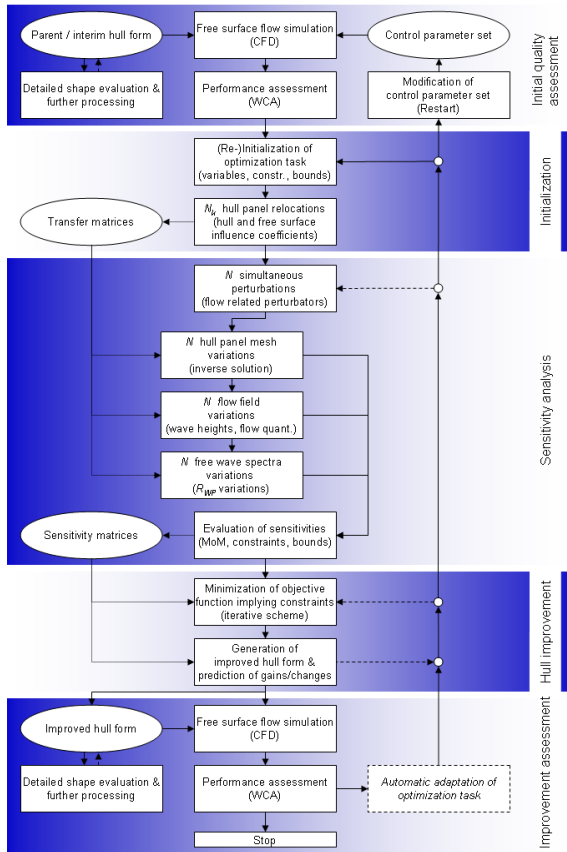


Fig. 1: Optimization process flow.

firm convergence. The computed wave elevations (longitudinal wave cut) are then passed to the longitudinal wave cut analysis which provides the free wave spectra and the wave pattern resistance. The free surface flow solution along with the wave spectra and the wave pattern resistance serve as the base solution for the sub-optimization task. Details are given in section 3

**Initialization** The optimization variables (the flow related perturbators) are set, the constraints and bounds are determined. A systematic hull panel perturbation is conducted which yields the transfer matrices. Transfer matrices measure the changes of the influence coefficients and induced velocities w.r.t predefined small relocations of the hull panel positions. They serve as the basic instrument for the sensitivity analysis. Details are given in section 4.

**Sensitivity analysis** Once assembled the transfer matrices are directly utilized to evaluate the impact of perturbation of the optimization variables (the perturbators) on the hull panel mesh in turn, on the flow field, on the wave formation and, finally, on the free wave spectra and the wave pattern resistance. As the consequence of the linear perturbation approach all these impacts are determined for all optimization variables in parallel straightforward by simple scalar matrix multiplications. The impacts of perturbation are compiled in terms of sensitivity matrices for the objective function and the constraints (bounds). Details are given in section 4.

**Hull improvement** The sensitivity matrices are passed to the hull improvement instance. Here the objective functional is set up in terms of a convex sum of the objective function and weighted constraints terms (least-squares formulation) and the optimum – the minimum – is determined within the perturbation scope of the sub-optimization task by iterative solution of the governing equation system. The iteration is applied to gradually isolate active from passive constraints, see section 5.

Having determined the optimal variable set, an improved hull form is derived again applying the sensitivity matrices. The hull form is obtained in terms of a smoothly relocated hull panel mesh which possesses the same topology as the initial mesh. Details are given in section 5.

**Improvement assessment** Finally, the improved hull geometry is sent to the hydrodynamic analysis providing the wave spectra and the wave pattern resistance which serves, along with the improved hull form (usually the associated point grid of the hull panel mesh), as the base point (base solution) for the next sub-optimization loop.

Formally, a sub-optimization task is composed of a prediction and a correction step. The prediction step, essentially, comprises the initialization, the sensitivity analysis and the hull improvement stage. In the correction step the predicted improvements are assessed by a flow and wave cut analysis. Here, the predicted optimization results are 'corrected' or updated for nonlinearities, for the new dynamic floating position and for deviations potentially caused by the reconstruction of a coherent hull surface from a relocated hull panel mesh.

The optimization process terminates if a stopping

criterion becomes active. Otherwise, the optimization enters the next sub-optimization loop. Even though the entire process is fully automated requiring no user interaction, the user may manually interrupt the process at certain points. This allows, for instance, to restart from any previous solution with a modified or adapted set of control parameters.

### 3 Hydrodynamic analysis

Advanced, reliable and fast CFD tools based on inviscid potential theory are widespread and are the first choice in practical wave resistance computation and optimization for a wide range of ship types and flow cases. Here the flow analysis is conducted by the free surface Rankine panel module XSPAN of the CFD system SHIPFLOW, FLOWTECH Int. AB., see Larsson (1997) and Janson (1997)

Most of the CFD codes utilize integral resistance values derived from hull pressure integration. In this way, however, information is lost on where beneficial and adverse effects originate. In the present context longitudinal wave cut analysis is applied to the computed wave pattern both in the sense of system identification and to provide the objective function of optimization. Wave cut analysis yields the wave pattern resistance  $R_{WP}$  while – by convention – hull pressure integration provides the wave resistance  $R_W$ .

#### 3.1 Free surface potential flow

The boundary value problem of free surface potential flow is thoroughly discussed and documented in the literature, e.g. Janson (1997), and is addressed here only in short.

A right-handed Cartesian system is defined, see figure 2, which is fixed to the ship having the same speed but does not follow its dynamic trim and sinkage. The quantities in this section are non-dimensionalized by the onset flow  $|\vec{U}_\infty|$  and/or the ship length between perpendiculars  $L_{PP}$ .

The governing equation of free surface potential flow is the Laplace equation which is derived from mass continuity. Assuming an inviscid (ideal) incompressible fluid with irrotational flow, the velocity components can be determined from the gradient of the total velocity potential  $\phi$  which comprises

the potential of the undisturbed onset flow  $\phi_\infty$  and the disturbance potential  $\phi'$  due to the ship

$$\phi = \phi_\infty + \phi' \quad (1)$$

The velocity potential has to satisfy the Laplace equation and it has to comply with the boundary conditions.

The kinematic hull boundary condition implies that the flow velocity must have a known component in the hull normal direction which is directed into the fluid since no fluid particle is supposed to pass through the surface of a rigid body. In terms of the disturbance potential the kinematic hull boundary condition reads

$$\frac{\partial \phi'}{\partial n} = -\hat{U}_\infty \cdot \vec{n} + F, \quad (2)$$

where  $\hat{U}_\infty = \vec{U}_\infty / |\vec{U}_\infty|$  indicates the unit velocity vector of the undisturbed onset flow. Usually  $F$  vanishes, since no fluid particle is supposed to pass through the surface of a rigid body. An additional dynamic hull boundary condition is imposed, claiming equilibrium between the hydrodynamic and hydrostatic pressure forces on the wetted hull portion and the ship's weight distribution. This integral condition primarily determines the dynamic trim and sinkage.

At the free surface two more boundary conditions are applied, both need to be fulfilled at the initially unknown wavy free surface. The kinematic free surface condition implies that the flow must be tangential to the free surface, i.e., no fluid particle is supposed to leave the surface  $\zeta = f(x, y)$ ,  $\zeta$  being the wave elevation (normalized). The second condition, the dynamic free surface boundary condition, states that the static pressure, expressed through Bernoulli's equation, must be constant (atmospheric) at the free surface.

The free surface problem is nonlinear since the free surface boundary conditions are nonlinear in the unknown velocity potential and are to be imposed at the initially unknown free surface. Solution methods for the fully nonlinear free surface flow have been proposed since the 1980s. Present methods linearize the free surface boundary conditions around a known base solution and solve the problem in an iterative manner. The majority of Rankine panel solvers adopt the so called Dawson or double-body flow linearization of the free surface boundary conditions.

Additional boundary conditions are required, e.g., to prevent waves from propagating upstream of the hull and to model the flow separation at the transom edge in case of ships possessing a transom stern.

The boundary value problem is solved numerically by distributing singularities, e.g. source singularities, on the boundaries of the flow domain, essentially the hull and the wavy free surface. Panel methods discretize the hull and a reasonable portion of the wavy free surface by quadrilateral (or triangular) panels. SHIPFLOW adopts (as one option) flat quadrilateral panels with a constant singularity distribution to approximate the boundary value problem. In their notation the flat quadrilateral panels are generated from so called input points which constitute a coherent point mesh along the hull. Input points are topologically equivalent to offset points which commonly are arranged along hull sections. In the original Hess & Smith method the flat quadrilateral panels are determined from the input points so that the panel corner points are at least a close approximation of the guiding input points (small gaps are inevitable introduced at the panel edges) and that the panel normal direction is a good approximation of the actual surface normal. The boundary conditions are enforced for each panel at a so called panel control point (or collocation point), usually, the panel's centroid.

As a consequence of the discretization the boundary value problem can be rewritten in terms of a set of equations, which yield an explicit relation for the unknown panel source densities  $\sigma_j$ :

$$\sum_{j=1}^{N_{FS}} \sigma_j A_{ij} = B_i \quad i \in [1, N_{FS}], \quad (3)$$

where  $A_{ij}$  indicates the influence coefficient from panel  $j$  to the velocity at panel  $i$ ,  $B_i$  is the inhomogeneous term at panel  $i$ .  $N_{FS}$  accounts for the total number of panels, including the hull and free surface panels. The influence coefficients  $A_{ij}$  are determined from the induced velocities  $X_{ij}$ ,  $Y_{ij}$  and  $Z_{ij}$ , which are pure geometrical quantities. They represent the induced portion from panel  $j$  to the velocity at panel  $i$  in the x-, y- and z-direction, respectively. At the free surface panels the velocities and velocity derivatives due to the base solution have to be considered in the influence coefficients, too. Details are given in Janson (1997).

The free surface domain is discretized by so called Rankine panels. The linearized boundary condition

is satisfied in a discrete sense at the free surface panel collocation points. Accordingly, the free surface elevation at collocation point  $i \in [N_H + 1, N_{FS}]$  ( $N_H$  denoting the total number of hull panels) is given by virtue of the linearized dynamic free surface boundary condition

$$\zeta_i = \frac{1}{2} F_n^2 [1 + \Phi_{xi}^2 + \Phi_{yi}^2 + \Phi_{zi}^2 - 2(\Phi_{xi} \phi_{xi} + \Phi_{yi} \phi_{yi} + \Phi_{zi} \phi_{zi})], \quad (4)$$

with the partial derivatives  $\Phi_x = \partial\Phi/\partial x$  etc.,  $\Phi$  being the velocity potential of the known base solution and  $F_n$  indicating the Froude number. The velocity at the  $i^{th}$  collocation point is determined from

$$\phi_{xi} = u_{xi} = \sum_{j=1}^{N_{FS}} X_{ij} \sigma_j + U_{\infty x}. \quad (5)$$

Similar expressions hold for the y- and z-directions.

Since the free surface condition is to be applied at the a priori unknown free surface an iterative solution scheme is used where (3) is solved successively. In each iteration the boundary value problem is linearized with respect to the solution of the previous iteration. Firm convergence is requested for the maximum wave change, for the maximum change of the source densities and, if allowed to freely adjust, for the ship's dynamic floating position which is updated via a force and momentum balance at each iteration.

The solution of the free surface boundary value problem is thoroughly described by Janson (1997).

### 3.2 Wave cut analysis

The steady ship wave system, as determined by means of a free surface potential flow computation, is further assessed by wave cut analysis. Wave cut analysis in the sense of system identification has shown to be a robust and powerful tool in CFD based optimization of the wave-making characteristics of ships, e.g. Heimann (2000) and Heimann and Harries (2003). In the present scheme the longitudinal wave cut method is applied by means of a tool called SWASH (Ship Waves Analysis Light), see Heimann (2005) for details. Alternatively its re-implementation called FRIENDSHIP-Waves by FRIENDSHIP SYSTEMS (2006) might be applied. Both tools are adaptations of the wave cut method by Sharma (1966) and Eggers et al. (1967).

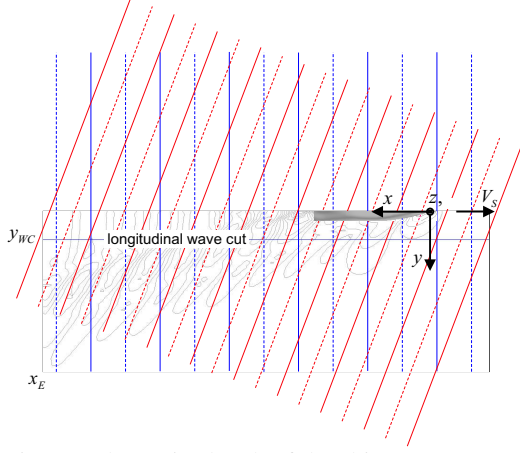


Fig. 2: Schematic sketch of the ship wave system (only one symmetric half is considered).

In case of flows symmetric to the ship center plane, a single (infinitely) long wave cut parallel to the ship suffices to perform the whole analysis. The longitudinal wave cut method was preferred to other wave analysis methods since it is comparatively fast, relatively robust in application and it has a broad application range (e.g. experimental investigations).

The ship's fixed reference coordinate system is the same as for the flow analysis, see figure 2. Yet, wave cut analysis is invariant with regard to the longitudinal position of the coordinate origin. Infinite water depth is assumed (but, in general, finite water depth has to be accounted for).

Essential assumptions of the method are ideal flow and the existence of so called 'free waves' at a sufficient distance from the ship. Formally, the wave pattern resistance can be deduced from conservation of momentum in a control volume which contains the steady ship wave system composed of a superposition of plane progressive waves of all feasible wave directions  $\theta$  and varying wave amplitudes in compliance with the steadiness condition for the phase velocity.

The wavenumber  $k$  and the wavelength  $\lambda$  are related by the dispersion relation

$$k(\theta) = \frac{2\pi}{\lambda(\theta)} = k_0 \sec^2(\theta), \quad (6)$$

with the basic wavenumber  $k_0$  and the fundamental wavelength  $\lambda_0$ , respectively, given by

$$k_0 = \frac{g}{V_S^2}, \quad \lambda_0 = \frac{2\pi}{k_0}, \quad (7)$$

$V_S$  being the ship speed and  $g$  the gravitational field strength.

The wave pattern resistance is computed from the sine and cosine components,  $A_S(\theta)$  and  $A_C(\theta)$ , respectively, of the free wave spectrum.  $A_S(\theta)$  and  $A_C(\theta)$  are linear functions of the Fourier transforms of the wave cut signal, for details see Heimann (2005). Even though  $A_S(\theta)$  and  $A_C(\theta)$  are frequently called wave amplitude functions they are better denoted as wave energy equivalents which measure the wave energy distribution along the components of the ship wave system. The free wave spectra are pure functions of the hull shape and the ship speed. This is why they are extremely valuable in ship hull optimization. Presently the free wave spectra are directly utilized for decision making in terms of the wave pattern resistance. The wave pattern resistance is computed by integration over the component waves  $\theta$

$$R_{WP} = \pi \frac{\rho g}{k_0^3} \int_0^{\pi/2} [A_S^2(\theta) + A_C^2(\theta)] \cos^3(\theta) d\theta, \quad (8)$$

$\rho$  being the water density. From (8) the wave pattern resistance coefficient follows by normalization according to

$$C_{WP} = \frac{R_{WP}}{0.5 \rho S_{ref} V_S^2} = \int_0^{\pi/2} C_{WP}(\theta) d\theta, \quad (9)$$

with  $S_{ref}$  denoting the wetted hull surface area for normalization. A useful and descriptive chart is obtained by plotting the integrand of (9) as a function of the component wave direction

$$C_{WP}(\theta) = \frac{2\pi}{S_{ref} k_0^2} [A_S(\theta)^2 + A_C(\theta)^2] \cos^3(\theta). \quad (10)$$

Expression (10) yields a valuable resistance functional which measures the wave energy distribution along the components of the ship wave system, see figure 8.

In practical applications due to limited computer resources in CFD simulations or restrictions due to tank wall reflections in model tests longitudinal wave cuts need to be truncated at a finite distance downstream of the hull. In order to retain the wave energy contained within the wave pattern downstream of the truncation point SWASH

(and FRIENDSHIP-Waves) treats wave cuts of finite length with a special truncation correction. At a sufficiently large distance aft of the stern the wave cut is usually dominated by transverse waves following the ship. This gives rise to utilizing an analytic truncation function composed of harmonic waves decaying to infinity. A truncation correction based on an analytical asymptotic extension of the wave cut is applied here.

Sharma (1966) and Eggers et al. (1967) suggested the following approach for an analytical asymptotic extension of the wave cut infinitely downstream

$$\tilde{\zeta}(x, y) \Big|_{x_E+} \simeq \frac{c_1 \cos(x) - c_2 \sin(x)}{\sqrt{c_3 + x}} \quad x \rightarrow +\infty, \quad (11)$$

where the coefficients  $c_1$ ,  $c_2$  and  $c_3$  are determined by fitting (11) to the tail end of the wave cut signal up to the truncation point  $x_E$ . The unknown coefficients are determined by regression analysis. Because of the strong asymptotic decay of both the wave elevation and the slope at  $x \rightarrow -\infty$  no correction is performed for the truncation of the wave cut upstream.

The contribution of the truncation correction to the overall wave pattern resistance, finally, can be evaluated in closed analytical form.

The application of longitudinal wave cut analysis mainly depends on the ship's speed, on the lateral position of the cutting plane and on the utilizable length of the wave signal up to the truncation point  $x_E$ . According to the author's experience satisfactory results are obtained for medium speed and fast ships at lateral cut positions in the range  $0.2 \leq y/L_{PP} \leq 0.25$  provided the cut extends far enough downstream to allow for a reasonable truncation correction.

## 4 Sensitivity analysis

The sensitivity analysis and the hull form improvement are the central units of the optimization process as discussed in section 2. The sensitivity analysis comprises the cause and effect chain from the variation of the optimization variables (the cause) to the variation of the wave pattern, the free wave spectra and the wave pattern resistance (the effects). The sensitivity chain is simplified by linear perturbation of the boundary value problem around its actual state. By application of the perturbation ap-

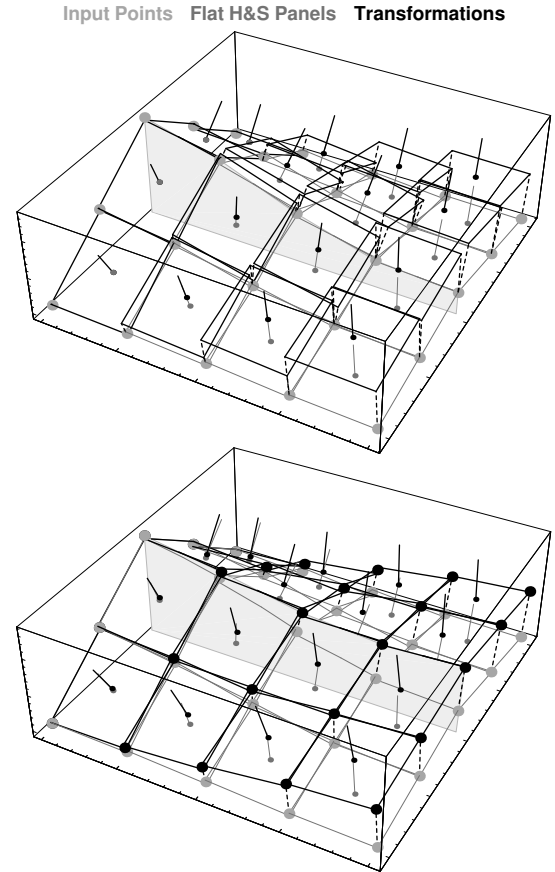


Fig. 3: Fitting of a transom wedge (upside down); top: stepped hull panel normal relocation, bottom: effect of joint relocation.

proach the nonlinear relations are transferred to explicit equations depending in a linear and straightforward manner on the optimization variables. This way, costly direct numerical solutions by means of CFD for a large set of variables are avoided.

Commonly, the design variables in ship hull form optimization are directly related to the hull geometry definition (offsets, polynomial shift functions, spline vertices or even higher level geometry descriptors like hull form parameters). In this way, however, the optimization and its outcome inevitably are constrained by the characteristic features of a specific geometric hull definition (which might be desired in certain applications). In the present approach optimization control is attained via local flow related perturbators which are directly related to the discretization of the flow problem. This permits a more self-contained hull vari-

ation which is decoupled and, hence, independent from a geometric definition of either the shape or its modifications.

The hull panel source densities (perturbators) of the potential flow solution are used to establish the natural link between hull and flow field variations. Coupling the source densities and the discretized hull surface, represented by a mesh of flat quadrilateral panels, is attained via the linearized kinematic boundary condition which is to be fulfilled at all time (see below). Consequently, each hull panel source density variation requires a corresponding relocation of the hull panel mesh itself (in a desingularized method a relocation of the control point) and vice versa. In the present scheme the panel mesh relocation is conducted by allowing the hull panels to shift normally to the hull, i.e., in their normal directions in- or outwards to the hull panel mesh. This was found to simulate a continuous hull surface 'deformation' in the most natural way. A variable (user defined) influence segment (of hull panels) around each perturbator controls the extension of each perturbation influence, i.e., from locally confined to spreading out across the entire hull panel mesh. Examples of panel mesh relocations are shown in figures 3 and 4.

The perturbation relations are derived by expanding both the panel source density variations and the variations of the panel mesh itself in terms of perturbation expressions which are then applied to the boundary value problem. A small parameter  $\varepsilon$  is introduced into the problem such that an already known  $0^{\text{th}}$ -order solution corresponds to  $\varepsilon = 0$  and that all higher order perturbations of this basic solution are traceable by their specific power of  $\varepsilon$ . The benefit of this approach is that any nonlinear problem can be decomposed into a sequence of linear problems with ascending order by sorting in powers of  $\varepsilon$ . The linear subproblems can then be solved separately one after the other. Yet, a restriction to the  $1^{\text{st}}$ -order problem already yields a meaningful approximation of the fully nonlinear problem, presuming the perturbation magnitude is kept 'small'. The approximation is known to get closer the smaller  $\varepsilon$  gets. For the hull panel source densities this yields

$$\begin{aligned}\sigma_n &= \sigma_n^{(0)} + \varepsilon \sigma_n^{(1)} + \mathcal{O}(\varepsilon^2), \\ \Delta \sigma_n &= \varepsilon \sigma_n^{(1)} + \mathcal{O}(\varepsilon^2) \quad n \in [1, N].\end{aligned}\quad (12)$$

Superscript  $(0)$  indicates the  $0^{\text{th}}$ -order solution, i.e.,

the basic solution which corresponds to a fully converged nonlinear free surface potential flow solution. Whereas  $(1)$  denotes the  $1^{\text{st}}$ -order solution, i.e., the perturbation expression.  $N$  is the number of hull panel source densities (perturbators) utilized in the optimization which usually is less than or equal to the total number of hull panels  $N_H$ .

In a perturbation sense the perturbation magnitudes  $\Delta \sigma$  must be 'small' compared, e.g., to the average of all hull panel source densities weighted by their respective panel areas  $S_i$

$$\Delta \sigma_n \equiv \Delta \sigma = \delta_\sigma \frac{\sum_{i=1}^{N_H} S_i |\sigma_i^{(0)}|}{\sum_{i=1}^{N_H} S_i}, \quad (13)$$

with  $0 < \delta_\sigma \ll 1$ . Definition (13) can be equivalently interpreted as an increment of the average volume flow through all hull panels. The advantage of definition (13) is that it accounts for the specific hull panelization and the flow case in question which allows a intuitive and appropriate choice of  $\Delta \sigma$ .

The corresponding perturbation of the hull panel mesh itself is

$$\begin{aligned}\vec{P}_k &= \vec{P}_k^{(0)} + \varepsilon \vec{n}_k^{(1)} + \mathcal{O}(\varepsilon^2), \\ \Delta \vec{P}_k &\equiv \Delta \vec{n}_k = \varepsilon n_k^{(1)} \hat{n}_k + \mathcal{O}(\varepsilon^2) \quad k \in [1, N_K],\end{aligned}\quad (14)$$

$\vec{P}_k$  denotes any point on the flat quadrilateral panel  $k$ , e.g., the control point.  $N_K (\leq N_H)$  is the number of active hull panels applied in the panel normal relocation scheme. The magnitude of the panel shift in panel normal direction is composed of the shift amplitude  $n_k^{(1)}$  and the unit vector normal  $\hat{n}_k$ .

The magnitudes of the hull panel relocations  $\Delta n$  may be related to a 'typical' hull panel size, e.g., the average hull panel diagonal or the average square roots of the hull panel areas  $S_i$

$$\Delta n_k \equiv \Delta n = \delta_n \frac{\sum_{i=1}^{N_H} \sqrt{S_i}}{N_H}, \quad (15)$$

with  $0 < \delta_n \ll 1$ . Again the advantage of such a definition is that it accounts for the specific hull panelization in terms of the panel mesh resolution allowing a good choice of  $\Delta n$ .

## 4.1 Sensitivity chain

The process chain of the sensitivity analysis is as follows:

- It commences with a firmly converged free surface potential flow solution, eq. (3), as basis.
- The computed wave field (4) is assessed by longitudinal wave cut analysis, eq. (8).
- Transfer matrices are determined to initialize the sensitivity analysis. The transfer matrices (19) and (22) store the changes of the influence coefficients due to the hull panel mesh perturbation (14).
- The effects of  $N$  hull source density perturbations (12) are determined. Utilizing the transfer matrices and in compliance with the linearized boundary value problem each hull panel source density perturbation directly modifies
- the hull geometry in terms of hull panel normal relocations (from inverse solution of (18)) in the neighborhood of the perturbator,
- the flow field, particularly, the wave elevations (21), and, finally,
- the free wave spectra (23) and the wave pattern resistance (24) which is assessed by wave cut analysis.

Above impacts of  $N$  hull source density perturbations are computed in parallel and straightforward by scalar evaluations and are compiled in terms of sensitivity matrices to be further used by the optimization instance.

## 4.2 Perturbation relations

The sensitivity chain is accessed by linear perturbation of the boundary value problem around its actual state.

The influence coefficients  $A_{ij}$ , the inhomogeneous term  $B_i$  and the induced velocities  $X_{ij}$ ,  $Y_{ij}$  and  $Z_{ij}$  in the governing flow equations (3), (4) and (5) depend in an implicit, nonlinear manner on the panel geometry and location. To make the dependencies explicit the influence coefficients and the induced velocities are expanded in Taylor series in  $n_k^{(1)}$  which, in the sense of the linear perturbation approach, are

truncated after the linear terms. This gives for  $A_{ij}$  ( $B_i$  accordingly)

$$\mathbb{A} \equiv A_{ij} = A_{ij}^{(0)} + \varepsilon \sum_{k=1}^{N_K} n_k^{(1)} \frac{\partial A_{ij}^{(0)}}{\partial n_k} + \mathcal{O}(\varepsilon^2), \quad (16)$$

with  $i, j \in [1, N_{FS}]$  and for the induced velocities (only the the free surface portion is required), e.g. the  $x$ -component  $X_{ij}$

$$\mathbb{X} \equiv X_{ij} = X_{ij}^{(0)} + \varepsilon \sum_{k=1}^{N_K} n_k^{(1)} \frac{\partial X_{ij}^{(0)}}{\partial n_k} + \mathcal{O}(\varepsilon^2), \quad (17)$$

with  $i, j \in [N_H + 1, N_{FS}]$ ; accordingly for  $Y_{ij}$  and  $Z_{ij}$ . Introducing equation (16) together with the perturbation approaches (12) and (14) to equation (3), neglecting higher order contributions of  $\mathcal{O}(\varepsilon^2)$  and finally sorting in orders of  $\varepsilon$  yields for the  $0^{th}$ -order again the basic equation system (3) and for the  $1^{st}$ -order the linear perturbation expression (in compact matrix notation)

$$\mathbb{A}^{(0)} \cdot \vec{\sigma}^{(1)} = -\mathbb{T}^{(0)} \cdot \vec{n}^{(1)}. \quad (18)$$

The transfer matrix  $\mathbb{T}^{(0)}$  is given by

$$\mathbb{T}^{(0)} \equiv T_{ik}^{(0)} = -\frac{\partial B_i^{(0)}}{\partial n_k} + \sum_{j=1}^{N_{FS}} \sigma_j^{(0)} \frac{\partial A_{ij}^{(0)}}{\partial n_k}, \quad (19)$$

with  $i \in [1, N_{FS}]$  and  $k \in [1, N_K]$ . Equation (18) represents the fundamental linear perturbation relation connecting the source density variations  $\vec{\sigma}^{(1)}$  and the panel normal relocations  $\vec{n}^{(1)}$ , see also Kraus (1989). The coefficient matrix  $\mathbb{A}^{(0)}$  is already known from the base flow solution. For the evaluation of the transfer matrix  $\mathbb{T}^{(0)}$  the changes of the influence coefficients with respect to the hull panel normal relocations have to be computed which can be done either analytically or numerically. Since the normal relocation of a single hull panel only affects a single row and a single column in the influence coefficient and induced velocity matrices a fast and memory conserving scheme was developed for the successive construction of the transfer matrices. Once the transfer matrices are compiled equation (18) is solved for varying right hand sides in a straightforward manner by LU-decomposition and back substitution. This is also known as the solution of the direct problem: finding the variation of the source densities in response to a perturbation of the hull panel mesh.

Principally, inversion of the transfer matrix in (18) yields the solution of the inverse design problem which is required in the proposed scheme to determine for each source density (perturbator) variation its correlative hull panel mesh relocation. Inversion of the transfer matrix requires special precautions with regard to the dimensionality of the problem, details are given in Heimann (2005).

Having determined the hull panel mesh relocations from the inverse solution of (18) the associated perturbations of the principal hydrostatics like displacement volume, center of buoyancy, center of flotation and the waterline area are predicted from respective linearized perturbation relations in a discrete sense based on the information of the distorted hull panel mesh (under the wavy free surface of the advancing ship). In principle, the denser the hull panelization the more accurate is the prediction, for an elaboration see Heimann (2005).

The perturbation impact on the flow field, particularly, on the wave elevation is given as the sum of the basic wave elevation  $\zeta^{(0)}$  and its variation  $\Delta\zeta$

$$\zeta(x,y) = \zeta^{(0)}(x,y) + \Delta\zeta(x,y) . \quad (20)$$

The perturbation portion is derived from the dynamic free surface boundary condition (4) which, by virtue of equations (5), (17) and the perturbation approaches (12) and (14), again neglecting higher order contributions of  $\mathcal{O}(\varepsilon^2)$  and sorting in orders of  $\varepsilon$ , yields for the  $0^{th}$ -order again the basic free surface condition (4) and for the  $1^{st}$ -order the linear perturbation expression for the wave elevations at the free surface collocation points

$$\Delta\vec{\zeta} = -F_n^2 \left[ \vec{U}_x \left( \mathbb{X}^{(0)} \cdot \vec{\sigma}^{(1)} + \mathbb{T}_{\mathbb{X}}^{(0)} \cdot \vec{n}^{(1)} \right) + \vec{U}_y \left( \mathbb{Y}^{(0)} \cdot \vec{\sigma}^{(1)} + \mathbb{T}_{\mathbb{Y}}^{(0)} \cdot \vec{n}^{(1)} \right) + \vec{U}_z \left( \mathbb{Z}^{(0)} \cdot \vec{\sigma}^{(1)} + \mathbb{T}_{\mathbb{Z}}^{(0)} \cdot \vec{n}^{(1)} \right) \right] . \quad (21)$$

$\vec{U}_{x,y,z}$  are the velocities according to the last iteration step previous to the converged base  $^{(0)}$  free surface flow solution.  $\mathbb{T}_{\mathbb{X}}^{(0)}$ ,  $\mathbb{T}_{\mathbb{Y}}^{(0)}$  and  $\mathbb{T}_{\mathbb{Z}}^{(0)}$  are the transfer matrices for the change of wave elevation. The  $x$ -component reads

$$\mathbb{T}_{\mathbb{X}}^{(0)} \equiv T_{X ik}^{(0)} = \sum_{j=1}^{N_{FS}} \sigma_j^{(0)} \frac{\partial X_{ij}^{(0)}}{\partial n_k} , \quad (22)$$

with  $i \in [N_H + 1, N_{FS}]$  and  $k \in [1, N_K]$ ;  $\mathbb{T}_{\mathbb{Y}}^{(0)}$  and  $\mathbb{T}_{\mathbb{Z}}^{(0)}$  follow accordingly. The transfer matrices comprise the changes of the induced velocities at the free surface due to the hull panel normal relocations and are evaluated simultaneously together with equation (19) by a fast and memory conserving scheme in the initialization step.

Finally, the perturbation impact on the free wave spectra and the wave pattern resistance is computed straightforward by Fourier transformation (wave cut analysis) of the superimposed wavy free surface (20). This yields for the free wave spectra, in perturbation sense, the sum of the basic wave spectra  $A_S^{(0)}$  and  $A_C^{(0)}$  and their variations  $\Delta A_S$  and  $\Delta A_C$

$$\begin{aligned} A_S(\theta) &= A_S^{(0)}(\theta) + \Delta A_S(\theta) , \\ A_C(\theta) &= A_C^{(0)}(\theta) + \Delta A_C(\theta) , \end{aligned} \quad (23)$$

which are deduced from Fourier transforms of the perturbation wave cut signal.  $\Delta A_S$  and  $\Delta A_C$  are linear functions of the perturbators  $\vec{\sigma}^{(1)}$ . Now, introducing the perturbation expressions (23) to the wave pattern resistance (8) yields the objective function of wave resistance optimization

$$\begin{aligned} f_{R_{WP}}(\vec{\sigma}^{(1)}) &= \\ &\int_0^{\pi/2} \left[ \left( A_S^{(0)}(\theta) + \Delta A_S(\theta) \right) \cos^{3/2}(\theta) \right]^2 d\theta + \\ &\int_0^{\pi/2} \left[ \left( A_C^{(0)}(\theta) + \Delta A_C(\theta) \right) \cos^{3/2}(\theta) \right]^2 d\theta . \end{aligned} \quad (24)$$

It reveals a quadratic dependency with respect to the wave spectra perturbations and hence to the optimization variables  $\vec{\sigma}^{(1)}$  (perturbators). The objective function (24), which inherently is of least-square type, is utilized as is directly in the optimization functional. Obviously, a reduction of the wave resistance can be achieved only by minimization of the free wave spectra sine and cosine components separately, weighted by  $\cos^{3/2}(\theta)$ .

## 5 Hull improvement

The optimization process is established in terms of successive sub-optimization loops (figure 1) which build on top of each other. In other words: each loop

utilizes the already improved hull of the predecessor loop. At each sub-optimization task a simplified convex quadratic image of the actual solution space in a 'trust-region' around the current base point (either the initial solution or those of the predecessor loop) is attained which is known to possess only one single minimum (uni-modal) determined by the active constraints.

The optimization functional, which is to be minimized, combines the objective function (24) and  $N_G$  optimization (inequality) constraints  $\bar{g}_j(\vec{\sigma}^{(1)})$  in terms of a positively weighted convex sum of least-square terms

$$F(\vec{\sigma}^{(1)}) = w_0 f_{RWP}(\vec{\sigma}^{(1)}) + \sum_{j=1}^{N_G} w_j \bar{g}_j(\vec{\sigma}^{(1)}). \quad (25)$$

$w_0 (> 0)$  may be any non-zero positive scaling factor and  $w_j (\geq 0)$  are either positive scalar weights indicating active constraints, or are vanishing in case of inactive constraints.

All optimization constraints are formulated in terms of inequalities. This way, freedom is introduced to the optimization task since boundary conditions do not need to be met exactly but rather have been relaxed to a certain band. For a consistent treatment of all constraint terms in (25) generalized inequality constraints are defined as

$$\bar{g}_j(\vec{\sigma}^{(1)}) = \left( \frac{C_j(\vec{\sigma}^{(1)}) - C_j^{(0)} - C_{j\text{shift}}}{\Delta C_{j\text{max}}} \right)^2 - 1 \leq 0, \quad (26)$$

which are related to their respective maximum bounds  $\Delta C_{j\text{max}} (> 0)$ , for all  $j \in [1, N_G]$ . Thus, a certain penalty is introduced to the objective function as soon as a constraint becomes active. The magnitude of the penalty is controlled via its leading weight  $w_j$ .  $C_j(\vec{\sigma}^{(1)})$  is the actual constraint value (due to perturbation),  $C_j^{(0)}$  indicates the base value (before perturbation) which is required to be inside the bounds and  $C_{j\text{shift}}$  a center-shift of the  $j^{\text{th}}$  constraint to allow for asymmetric positioning of the boundaries with respect to  $C_j^{(0)}$ . Active constraints directly lie on their bound or are outside the bounds, whereas, inactive constraints stay within the permissible range.

Constraints are applied to the hull panel normal relocations which must not exceed their perturbation bounds (at each sub-optimization loop), the latter

being defined according to equation (15). The same applies to the optimization variables  $\vec{\sigma}^{(1)}$  themselves, the maximum perturbations being limited by (13). Usually, the flat of bottom and flat of side are kept during optimization by treating the corresponding hull panels as passive or frozen. Furthermore, the displacement volume, the centers of buoyancy and flotation and the waterline area which are derived from the aggregated hull panel mesh relocations (the simultaneous effect of all local hull perturbations  $N$ ) are forced to stay within user defined bounds. Additional constraints have been introduced to keep track of adjacent relative hull panel relocations in order to ensure smooth transitions in the distorted panel mesh. Otherwise, normal relocations of adjacent hull panels in different directions or with different magnitudes may cause considerable gaps in the panel mesh, like in the exaggerated example in figure 3 (top). In total more than 5000 constraints need to be utilized in the optimization functional assuming an average scenario of about 1000 hull panel perturbations.

The first order necessary conditions for the minimum of the objective functional (25) require that the partial derivatives of  $F(\vec{\sigma}^{(1)})$  with respect to all optimization variables vanish

$$\vec{\nabla}_{\sigma^{(1)}} F(\vec{\sigma}^{(1)}) \stackrel{!}{=} \vec{0}, \quad (27)$$

with  $\vec{\nabla}$  denoting the Nabla-operator in vector notation. Partial differentiation yields the equation system for the  $N$  unknown optimization variables  $\vec{\sigma}^{(1)}$

$$\mathbb{M} \cdot \vec{\sigma}^{(1)} = \vec{B}, \quad (28)$$

The  $N \times N$  system matrix  $\mathbb{M}$  is symmetric, non-sparse but diagonally dominated and non-singular.  $\vec{B}$  comprises the inhomogeneous terms.

The solution of equation system (28) primarily depends on the appropriate choice of the weights  $w_j$  to distinguish active and inactive constraints. The minimum of (25) is determined solely by the active constraints, inactive constraints vanish. Since the appropriate weights are not known a priori they are iteratively adapted keeping track of the active set of constraints. In each such 'inner' iteration (28) is set up and solved for a new set of weights (commonly unity weights at the first iteration). The iteration terminates if the process has converged to the actual (feasible) minimum of the sub-optimization problem. The constraints weights at the 'inner' iter-

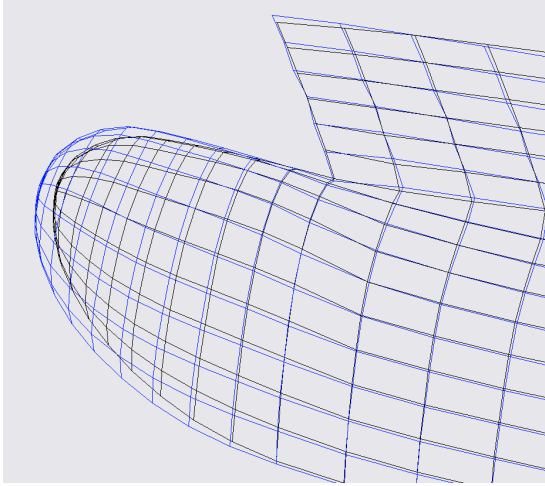


Fig. 4: Hull panel mesh relocation (blue) in the bulbous bow area due to optimization.

ation step  $i + 1$  are updated according to

$$w_j^{i+1} = w_j^i + r_f w_j^i \bar{g}_j^i(\vec{\sigma}^{(1)}), \quad (29)$$

with  $0 \ll r_f \leq 1$  occasionally applied to stabilize the iteration by under-relaxation. Constraints (weights) meanwhile dropped from the iteration procedure but which happen to become active in a subsequent iteration step are compelled to reenter the process, for details see Heimann (2005).

Even though the cost of setting-up and solving (28) increases disproportionate with the number of the optimization variables, in practical application cases with 1000-2000 variables, the iteration scheme is quite fast and memory conserving.

## 5.1 Hull form adaptation

Having computed the optimal set of variables, i.e., the variation of the hull panel source densities  $\vec{\sigma}^{(1)}$ , the improved hull form according to the actual process state (sub-optimization loop) is generated. The inverse solution of (18) yields the corresponding superposition of all local panel relocations which brings about a global hull variation in terms of a relocated hull panel mesh.

The new hull panel mesh still features small gaps between adjacent hull panels imposed by the relocation approach. A generalized example is given in figure 3 (top) by an over-pronounced panel mesh normal relocation. Even though smooth transitions

in the distorted panel mesh are already incorporated by the optimization further treatment of adjacent hull panels is required to restore a unique hull surface from the emerging incoherent panel cluster. A so called joint relocation scheme was invented to reconstruct a smooth point grid with a well defined topology from the relocated hull panel mesh by vector averaging of the bordering panel normal shifts (usually  $\leq 4$ , at symmetry planes up to eight) to the associated input point grid. An important aspect of the averaging procedure is to retain the characteristic of the relocated hull panel mesh as well as possible to realize a close match between the improvement prediction and its assessment (correction). Applications of the joint panel relocation are shown in figure 3 (bottom) and 4. For details on the joint relocation scheme see Heimann (2005).

The point mesh may either be used directly in terms of an offset description for a subsequent sub-optimization task or it may be further processed by surface interpolation or approximation techniques with CAX tools as, for instance, provided by FRIENDSHIP SYSTEMS (2006).

## 6 Applications

The potential of the optimization method is outlined by means of two test applications, both ships operate around  $F_n = 0.3$ . One is the well known and widely used double-symmetric Wigley hull, the second a state of the art twin screw ferry – the FANTASTIC FantaRoRo – typical of fast short-sea shipping featuring a bulbous bow and tunnelled transom stern. The FantaRoRo was devised as an elaborate test case within the European R&D project FANTASTIC, see Valdenazzi et al. (2003).

The Wigley hull was panelized (one symmetric half) by 605 hull panels (4482 panels at the free surface domain) with a slight stretching towards bow and stern. The wave pattern resistance was determined by longitudinal wave cut analysis utilizing SWASH. The wave pattern itself was computed by the nonlinear free surface Rankine panel module of the SHIPFLOW system. Thorough convergence was imposed for the wave elevations and for trim and sinkage.

All but the centerline hull panels were utilized for the hull perturbation. Only slight variations of about 1% in length and breadth were allowed. Displace-

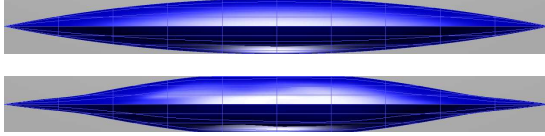


Fig. 5: Bottom view of the initial (top) and optimized (bottom) Wigley hull.

ment and waterplane area were relaxed to  $\pm 5\%$  of their initial values to give freedom to the optimization, the example having been chosen to illustrate the method. In total 11 successive sub-optimization loops were automatically performed by MinSWASH until the improvements in  $R_{WP}$  fall below a stopping criterium.

A substantial decrease of the wave making resistance by 49.4% was achieved. Both the displacement and the water plane area approach their lower bounds allowed within the optimization. The center of buoyancy experienced a slight forward shift of 0.23%  $L_{PP}$ . The hull outlines are compared in figure 5. Following optimization achievements led to a substantial reduction of the bow and stern/transverse waves (compare figure 6):

- The narrowed waterline angles at the entrance and run considerably reduce the bow and stern wave crests.
- The emerging shoulders (the initial hull neither features pronounced shoulders nor inflection points because of parabolic waterlines) are located at exactly half the fundamental wavelength resulting in a cancelation of the aft shoulder wave train.
- The fore shoulder wave train locates exactly one fundamental wavelength ahead of the stern wave system almost eliminating the latter.

Given a constraint minimization task, this is the expected result of the wave pattern resistance minimization for the Wigley hull. However, the augmented flow deflection at the shoulders may cause adverse viscous effects which were not studied here.

An application case of practical relevance is the FantaRoRo twin screw ferry which is taken to be a representative contemporary design. The main dimensions are:  $L_{PP} = 122.74$  m,  $B = 19.2$  m,  $T = 5$  m and  $C_P = 0.606$ . The Froude number of 0.311 corresponds to the service speed of 21 knots. The hull surface was discretized by 1166 (longitudinal

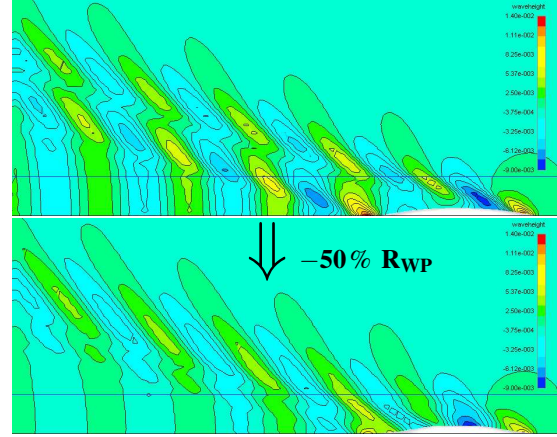


Fig. 6: Wave contours of the initial (top) and optimized (bottom) Wigley hull ( $F_n = 0.3$ ).

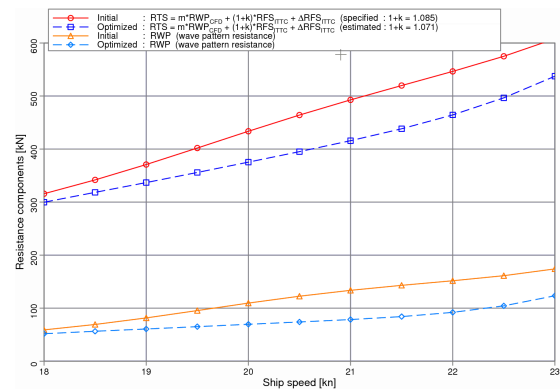


Fig. 7: Total resistance trial prediction (ITTC based) for the FantaRoRo (service speed 21 knots).

stretching towards bow and stern), the free surface by 4674 panels.

The optimization setup was very much the same as for the Wigley hull, again the bounds for displacement and waterplane being relaxed to  $\pm 5\%$ . (Typical optimizations usually are more restrictive.) All but the hull panels covering the flat of bottom and the stem profile, which were frozen during optimization, were utilized for the hull perturbation ( $> 1000$ ). In total 17 successive sub-optimization loops were conducted in automatic manner with ample convergence of the leading measures already within 15 loops.

The wave pattern resistance could be significantly reduced by 39.9%. Extrapolating the results to the trial condition (based on the ITTC method and a form factor assessment) yields a tangible reduction of the total resistance by 15.6% and of the resistance-displacement ratio by 11.3%, with the

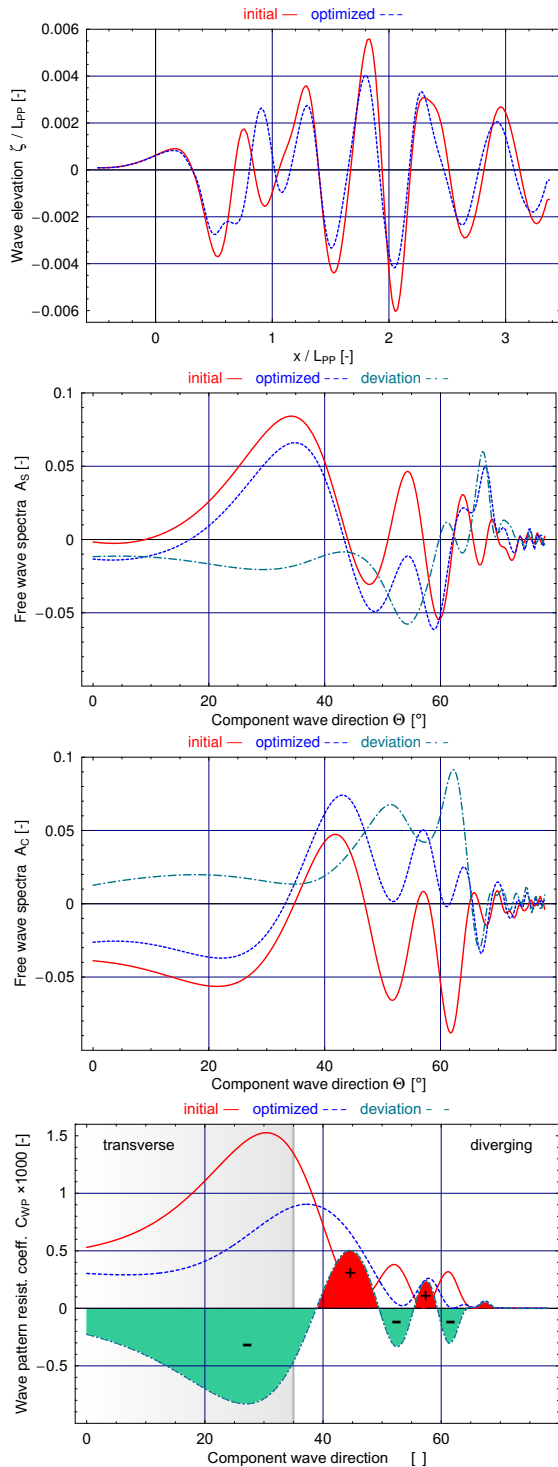


Fig. 8: Longitudinal wave cut at  $y/L_{PP} = 0.25$ , free wave spectra  $A_S$  and  $A_C$  and wave pattern resistance coefficient  $C_{WP}$  of the FantaRoRo.

improvements extending over a broad speed range, see figure 7. The distribution of wave energy in

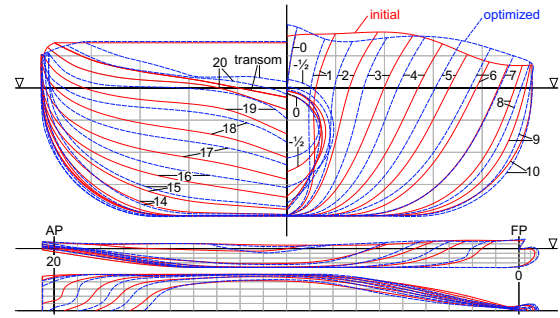


Fig. 9: Ship lines of the initial and optimized FantaRoRo.

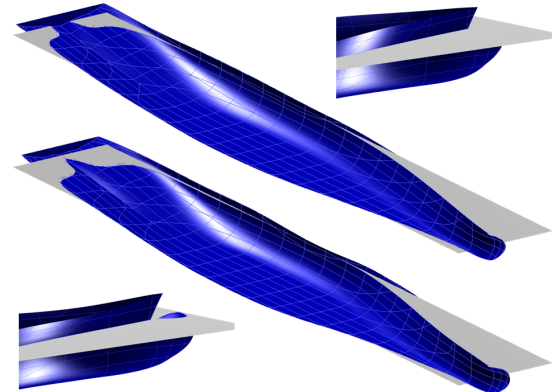


Fig. 10: Hull renderings of the initial (top) and optimized (bottom) FantaRoRo.

terms of  $C_{WP}$  along the components  $\theta$  of the wave system reveal the substantial reductions achieved in the transverse waves regime, particularly, in the stern wave system, see figure 8. Whereas, the gains and losses in the diverging waves are balanced. Both the displacement and the water plane area approach their lower bounds. The centers of buoyancy and flotation experienced a forward shift. Ship lines and hull renderings are presented in figures 9 and 10. In conclusion, the optimization achievements are (compare title figure showing the wave contours of the initial and optimized FantaRoRo ferry):

- The narrowed waterline entrance in conjunction with the increased down-flow at the bulb back reduce the bow and entrance waves.
- The bulbous bow wave crest and fore shoulder wave trough are positioned almost one fundamental wavelength apart generating a beneficial wave train interference.
- Evolving fore and aft shoulder wave troughs are

approximately half a fundamental wavelength apart resulting in a cancelation of the aft shoulder wave.

- The pronounced fore shoulder wave trough shifts aft which,
- in conjunction with the leveled transom flow separation, efficiently eliminates the stern wave system.

Within the optimization viscous flow effects were not taken into account. Therefore it is likely that the hull will not yield the full benefit as predicted with potential flow theory.

## 7 Summary

A novel hull form optimization approach is presented. It builds on inviscid, potential flow simulations of the ship wave pattern, on straightforward realization of the cause and effect relation of hull variations and their impact on wave formation, which is accessed by a perturbation approach, and on wave pattern analysis which yields the objective function of optimization in terms of free wave spectra and the wave pattern resistance. These features are highly integrated and controlled by a fully automated, self-governed optimization environment called MinSWASH to improve the ship's wave-making characteristics accompanied by a substantial reduction of the resistance and power consumption. Lying outside the focus of the present work, viscous dominated properties like the propulsive efficiency of the optimized hulls needs to be further assessed either by CFD or EFD.

In particular, the following has been shown:

- The wave-making characteristics could be considerably improved with a substantial reduction of the wave (pattern) resistance by up to 50%.
- Hull variations are driven by a flow related quantity to meaningful optimum hull shapes with the hull geometry fully self-adjusting according to the optimization requirements.
- Optimal interferences of local wave trains are enforced both in amplitude and phase which results in a beneficial cancelation of the wave trains.
- The specific fingerprints of locally confined hull variations can be effectively traced in the wave

spectra and in the wave pattern resistance to allow a focused minimization of particular adverse wave components.

- This significantly improves the system identification since the additional information in terms of the wave spectra and the distribution of the wave pattern resistance over the waves range are directly utilizable as objective function.
- Linear perturbation of the boundary value problem proved to be a valuable method of accessing nonlinear relations. Thus, fast and straightforward evaluation of the sensitivities of the objective function and the constraints is enabled, allowing a simultaneous treatment of numerous, locally acting optimization variables which introduces a high degree of freedom to the hull variation.
- The entire optimization process can be effectively established in terms of an iterative marching scheme of successive sub-optimization loops, each mapping (as a consequence of linear perturbation) the solution space to a simplified convex quadratic image, the sub-optimization space, which merely possesses a single minimum determined by the active constraints.

The outlined approach was already successfully applied to customer optimization projects at FRIENDSHIP SYSTEMS GmbH. Further development and integration is underway such as coupling the established parametric and the novel method advantageously.

It should be pointed out that highly developed hull lines naturally do not possess the potential of 50% reduction in wave resistance. However, the reduction of total resistance by 2-6% is regularly achievable, see Harries et al. (2006).

## 8 Acknowledgments

The presented research is based on the authors Ph.D. work which was primarily undertaken at the Division of Naval Architecture and Ocean Engineering of the Technical University Berlin and at FRIENDSHIP SYSTEMS GmbH.

## 9 References

- Birk, L.; Harries, S.** (2000) *Automated Optimization – A Complementing Technique for the Hydrodynamic Design of Ships and Offshore Structures*, 1st Int. Conf. on Computer Applications and Information Technology in the Maritime Industries (COMPIT 2000), Potsdam, Germany.
- Dudson, E.; Harries, S.** (2000) *Hydrodynamic Fine-Tuning of a Pentamaran for High-Speed Sea Transportation Services*, 8th Int. Conference on Fast Sea Transportation (FAST 2005), St. Petersburg, Russia.
- Eggers, K.W.H.; Sharma, S.D.; Ward, L.W.** (1967) *An Assessment of Some Experimental Methods for Determining the Wavemaking Characteristics of a Ship Form*, SNAME Trans., Vol. 75.
- FRIENDSHIP SYSTEMS** (2006) *FRIENDSHIP-Modeler, -Equi, -Flow, -Optimizer, -Waves – Users Manuals*, Rel. 0611xx, FRIENDSHIP SYSTEMS GmbH, Potsdam, Germany.
- Harries, S.; Abt, C.; Heimann, J.; Hochkirch, K.** (2006) *Advanced Hydrodynamic Design of Container Carriers for Improved Transport Efficiency*, Int. Conference on Design and Operation of Container Ships (RINA 2006), London, U.K..
- Heimann, J.** (2000) *Application of Wave Pattern Analysis in a CFD Based Hull Design Process*, 3rd Int. Numerical Towing Tank Symp. (NuTTS 2000), Tjärnö, Sweden.
- Heimann, J.** (2005) *CFD Based Optimization of the Wave-Making Characteristics of Ship Hulls*, Dissertation (Ph.D. Thesis), Department of Naval Architecture and Ocean Engineering, Technical University Berlin, ISBN 3-89820-445-6, Germany.
- Heimann, J.; Harries, S.** (2003) *Optimization of the Wave-Making Characteristics of Fast Ferries*, 7th Int. Conference on Fast Sea Transportation (FAST 2003), Ischia (Gulf of Naples), Italy.
- Janson, C.E.** (1997) *Potential Flow Panel Methods for the Calculation of Free-surface Flows with Lift*, Ph.D. Thesis, School of Mechanical and Vehicular Engineering, Chalmers University of Technology, Göteborg, Sweden.
- Kraus, A.** (1989) *Methoden der Störungstheorie als Hilfsmittel für den interaktiven Entwurf von umströmten Körpern*, (in German), Dissertation (Ph.D. Thesis), Institut für Schiffs- und Meerestechnik, Technische Universität Berlin, Germany.
- Kumar, S.A.; Heimann, J.; Hutchison, B.L.; Fenical, S.W.**; (2007) *Ferry Wake Wash Analysis in San Francisco Bay*, Int. Ports Conference (PORTS 2007), American Society of Civil Engineers (ASCE), San Diego, CA, USA.
- Larsson, L.** (1997) *SHIPFLOW User's Manual and Theoretical Manual*, FLOWTECH Int. AB, Göteborg, Sweden.
- Maisonneuve, J.-J.; Harries, S.; Marzi, J.; Raven, H.C.; Viviani, U.; Piippo, H.** (2003) *Towards Optimal Design of Ship Hull Shapes*, 8th Int. Marine Design Conf. IMDC'03, Athens, Greece.
- Sharma, S.D.** (1966) *An Attempted Application of Wave Analysis Techniques to Achieve Bow-Wave Reduction*, 6th Symp. on Naval Hydrodynamics, ONR/ACR-136, Washington D.C., USA.
- Söding, H.** (2001) *Resistance Decrease by Computer-Aided Hull Shape Improvements*, 2nd Int. Conference on High-Performance Marine Vehicles (HIPER 2001), Hamburg, Germany.
- Valdenazzi, F.; Harries, S.; Janson, C.-E.; Leer-Andersen, M.; Maisonneuve, J.-J.; Marzi, J.; Raven, H.C.** (2003) *The FANTASTIC RoRo: CFD Optimisation of the Forebody and its Experimental Verification*, Int. Conf. on Ship and Shipping Research (NAV 2003), Palermo, Italy.
- Valorani, M.; Peri, D.; Campana, E.** (2003) *Sensitivity Analysis Methods to Design Optimal Ship Hulls*, Optimization and Engineering, Vol. 4, pp. 337-364.